AN ALUMINUM NITRIDE PIEZOELECTRIC MICROPHONE FOR AEROACOUSTICS APPLICATIONS

M. D. Williams, B. A. Griffin, A. Ecker, J. Meloy, M. Sheplak[*]
Interdisciplinary Microsystems Group, Dept. of Mechanical and Aerospace Engineering,
University of Florida, Gainesville, Florida, USA

ABSTRACT

This paper describes an aluminum nitride (AlN)-based piezoelectric MEMS microphone designed to serve as aircraft fuselage instrumentation for full-scale noise characterization flight tests. The optimal microphone design was determined using lumped element modeling and composite plate theory. Measurements of the microphone's frequency response and linearity revealed it to have a higher sensitivity (71 µV/Pa), larger dynamic range (29 – 147 dB) with lower noise floor, and significantly higher resonant frequency (89 kHz) than previous piezoelectric aeroacoustic microphones.

INTRODUCTION

With the worldwide airline fleet estimated to double in the next 20 years [1], aircraft manufacturers increasingly face regulatory and market driven pressures to reduce aircraft noise. Passenger expectations for a quiet flight experience and concern about long-term noise exposure of flight crews are important drivers in aircraft manufacturers' efforts to reduce cabin noise in flight [2-3]. Treating the noise at its source shows potential for reduction of noise and weight savings compared to alternatives such as insulting panels.

In order to identify noise sources and assess the impact of noise reduction technologies during the design process, aircraft manufacturers require robust, low cost microphones. Measuring primary sources of cabin noise is difficult under simulated cruise conditions in test facilities [2] and establishes the need for microphones that can be used in full-scale tests at altitude. Their use on the fuselage exterior requires extremely small packaged sizes. Important performance metrics include a high maximum sound pressure level (SPL) ~150 dB coupled with a noise floor < 45 dB (ref 20 µPa/$\sqrt{Hz}$) and a flat frequency response in the audio band (~20 Hz – 20 kHz). Microelectromechanical systems (MEMS) microphones show promise for meeting the stringent performance requirements of aircraft manufacturers at reduced size and cost, made possible using batch fabrication technology.

Piezoelectric MEMS microphones, in particular, are a robust and less power-demanding alternative to capacitive or piezoresistive microphones. In the past, piezoelectric materials used in MEMS microphones have largely been lead zirconate titanate (PZT) and zinc oxide (ZnO) [4-10]. In contrast, the microphone presented here makes use of aluminum nitride (AlN), which provides inherent advantages in CMOS compatibility, dielectric loss, and signal-to-noise ratio [11]. Despite these advantages, the difficulty of aluminum nitride fabrication has led to few piezoelectric MEMS microphones using AlN [12-13], and those have not targeted aeroacoustic applications.

In this paper, a batch-fabricated AlN piezoelectric microphone designed to serve as aircraft fuselage instrumentation for full-scale noise characterization flight tests is presented. Microphone design and characterization are both addressed, and its performance is compared to previous piezoelectric MEMS microphones.

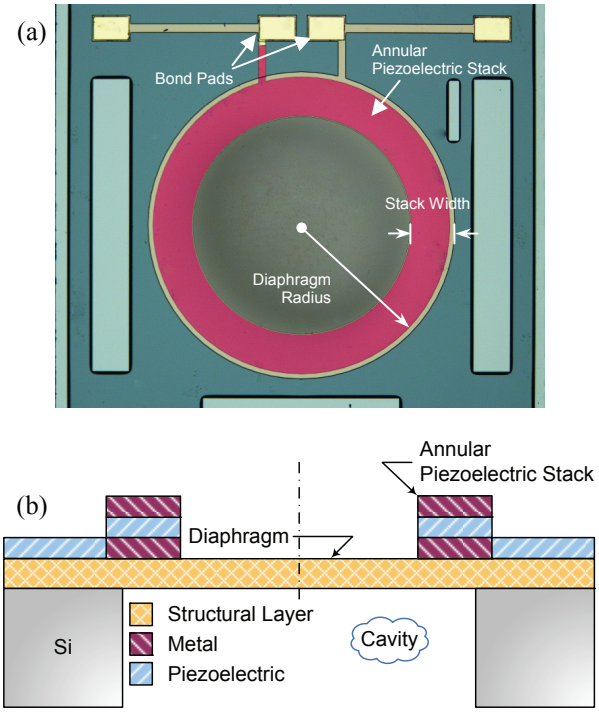

Figure 1. (a) Partial photograph of a piezoelectric microphone die (total die size is 2x2 mm^2); (b) Cross-sectional view of the microphone structure.

DESIGN

Structure

The microphone structure (Figure 1) includes a circular diaphragm composed of a structural layer and an annular piezoelectric/metal film stack, all deposited on a silicon substrate. As the diaphragm deflects under an incident acoustic pressure, strain in the piezoelectric yields an electric field that is sensed as a voltage difference across the metal electrodes. The location of the piezoelectric ring was chosen to take advantage of the high stress boundary region and to avoid the need for metal lines over the diaphragm surface. Diaphragm motion is enabled by an air cavity on the diaphragm backside.

Modeling

Lumped element modeling [14] is an effective technique for producing system-level transducer models via "lumping" of system components into equivalent mass-spring-damper elements. The use of lumped element modeling requires characteristic length scales of the transducer to be much smaller than the wavelength of associated physical phenomenon; for example, at frequencies of interest, the diaphragm dimensions must be much less than the wavelength of the incident acoustic pressure and the bending wavelength within the diaphragm itself. Using a circuit analogy to represent the lumped element model allows engineers to leverage intuitive understanding of circuit diagrams and available circuit analysis tools. In addition, the equivalent circuit model can be

coupled directly to additional circuitry, providing a true system-level model.

Figure 2(a) shows the microphone structure with associated lumped circuit elements. The diaphragm is modeled as a lumped mass and compliance, M_{AD} and C_{AD}, respectively. Damping is included as a resistance, R_{AD}, and is estimated from prior devices of similar size and shape [10]. Coupling between the diaphragm and the air on the topside is modeled using a radiation mass M_{ADrad} and resistance R_{ADrad} estimated from a classical acoustics solution for radiation impedance seen by a piston in an infinite baffle. The cavity is modeled as a mass and compliance, M_{AC} and C_{AC}, respectively. The vent (not shown) is presented as a resistance R_{AV}. The electrical elements associated with the piezoelectric stack are the capacitance, C_{EB}, piezoelectric leakage path R_{EP}, and lead resistance R_{ES}. Each of these elements are connected into an equivalent circuit, shown in Figure 2(b), based on whether they share a common "effort" (pressure/voltage) or "flow" (volume velocity/current). The piezoelectric transduction is represented as a transformer with turns ratio ϕ_A that relates the acoustic and electrical energy domains on the left and right sides, respectively. With expressions for each of the lumped elements known [10,15], the sensitivity of the microphone $S = v_0/p$ [V/Pa] may be found directly from the circuit diagram of Figure 2(b).

Lumped elements associated with the diaphragm mass/compliance and piezoelectric transduction are the most difficult to compute and are based on a static piezoelectric composite plate model. The model [15,16] is found from the solution of the Kirchhoff plate equations in the inner and outer (annular) regions, with matching conditions on displacements and forces/moments applied at the interface and clamped boundary conditions applied at the exterior. Arbitrary in-plane stresses are included in the linearized governing equations [16]. In addition, a nonlinear version of the model is used to estimate the maximum pressure ($P_{\max}$) at which the microphone response remains linear.

The lower end of the microphone's dynamic range, the minimum detectable pressure (*MDP*), is predicted via a circuit noise model (Figure 3) derived from the equivalent circuit model (Figure 2(b)). In this model, thermal noise sources [14] are added at the location of dissipative elements (as voltage sources in series or current sources in parallel with perfect dissipative elements) and the output power spectral density, S_o^v [V^2/Hz] may then be found. Note the inclusion of a buffer amplifier and its own noise contributions. The *MDP* is then simply the input-referred voltage noise,

$$MDP = \sqrt{\int_{f_1}^{f_2} \frac{S_o^v}{|S|^2} df} \quad \text{[Pa]}. \tag{1}$$

Optimization

The goal of a microphone design is maximization of its operational range (both in terms of frequency and pressure) while minding the demands of a particular application. The bandwidth requirements of a microphone are usually well known, such as the range of human hearing (20 Hz-20 kHz). Maximum pressure levels of interest are also usually known, but improvement in the *MDP*, regardless of requirements, yields improved measurement resolution. As a result, it is natural to state the objective function

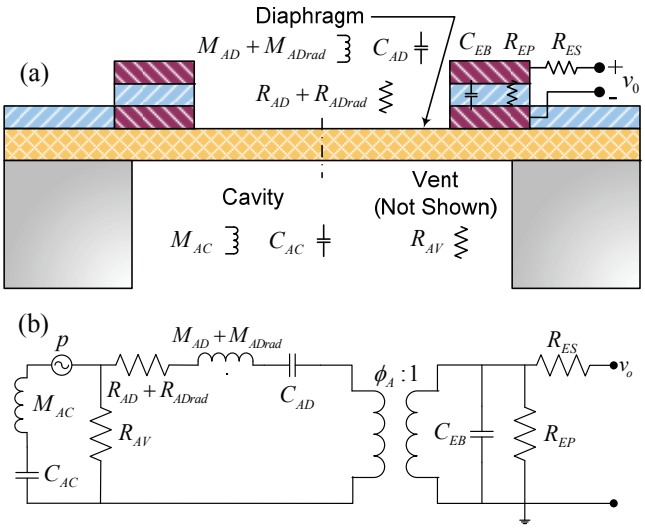

Figure 2. (a) Piezoelectric microphone structure with lumped circuit elements; (b) Equivalent circuit representation of a lumped element model of the piezoelectric microphone.

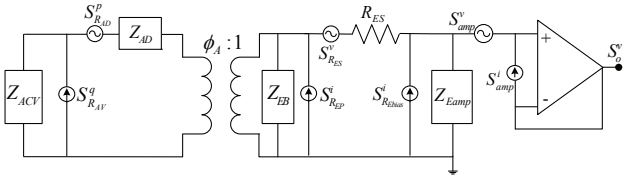

Figure 3. Microphone noise model including buffer amplifier.

for microphone optimization as

$$\min_{\overline{X}} \quad MDP\,, \tag{2}$$

where the design variables $\overline{X}$ include film thicknesses and radii. Constraints are placed on the bandwidth and $P_{\max}$, which are estimated from the equivalent circuit model and nonlinear composite plate model, respectively. Fabrication constraints (i.e. minimum radii, bounds on achievable film thicknesses, etc.) are also applied. The optimization yielded a diaphragm that was 1.3 µm in thickness with an outer diameter of 600 µm, an annular piezoelectric film stack width of 156 µm, and AlN thickness of 1 µm.

FABRICATION

Fabrication of the microphone was performed by Avago Technologies using a variant of their well-known FBAR process [13]. The proprietary process involves deposition and etching of the AlN and metal films followed by a backside deep reactive ion etch to define the cavity. At this time, sealing of the back cavity is accomplished at the packaging stage.

EXPERIMENTAL SETUP AND RESULTS

The first step toward characterization of the piezoelectric microphone was selection of the most promising microphone die. The voltage chirp excitation response of several microphones were inspected using a Polytec scanning laser vibrometer system, composed of a Polytec OFV 3001S vibrometer controller and OFV-074 microscope adapter attached to an Olympus BX600 microscope. Two of the microphones with resonant frequencies that compared favorably with the model (80 and 89 kHz, respectively, compared to 84 kHz predicted) were selected for further characterization. These microphones are described

throughout this section and are labeled Mic 1 and Mic 2, respectively.

Measurement of the sensitivity and linearity of both microphones was conducted in a normal incidence plane wave tube (PWT) using the Brüel & Kjær 4138 and PCB Piezotronics 377A12, respectively, as references. The PULSE Multi-analyzer system provided pseudo-random noise and single tone excitation signals for these measurements, which were amplified prior to rendering by a BMS compression driver at one end of the tube. The device under test (DUT) and reference microphone were mounted side-by-side at the end of the tube. The DUT was epoxied into a recess in a printed circuit board (Figure 5), which was clamped into position at the end of the plane wave tube via a slot in the backplate. BNC connections and appropriate electronics, including a buffer amplifier, were also located on this printed circuit board. The measurements were conducted over a 6.4 kHz bandwidth about a center frequency of 3.5 kHz with a 1 Hz bin width using 100 complex spectral averages. The maximum frequency of 6.7 kHz was dictated by the cut-on of higher order modes within the plane wave tube.

The microphone sensitivities are shown in Figure 6 together with the predicted value. The frequency responses were flat to within 1.5 dB and the sensitivity was 71 µV/Pa (-83 dB ref 1 V/Pa). The linearity measurement results in terms of total harmonic distortion for Mic 2 are found in Figure 7. Distortion was measured to be less than 2% up to 147 dB ref 20 µPa. Five harmonics of the fundamental tone f_1 = 1 kHz were considered in the calculation, i.e.

$$THD[\%] = 100\% \times \sum_{n=2}^{6} V^2(nf_1) / V^2(f_1) . \qquad (3)$$

Each of these five harmonics propagate as plane waves in the tube used for testing.

The sensor noise floors were also measured using a Stanford Research Systems SR785 spectrum analyzer, with the packaged microphones placed in a triple Faraday cage for shielding. Figure 8 shows the minimum detectable pressure, here calculated as the voltage noise spectra referred to the sensor input via the measured sensitivity at 1 kHz. Under these conditions, the noise floor for a 1 Hz bin centered at 1 kHz was measured to be 29 dB ref 20 µPa and the A-weighted noise floor was 64 dB ref 1 $Pa/\sqrt{Hz}$. Note that the 1/f shaped noise due to dielectric leakage in the piezoelectric extends into the audio band and that the sensor thermal noise floor is less than 20 dB ref 1 $Pa/\sqrt{Hz}$.

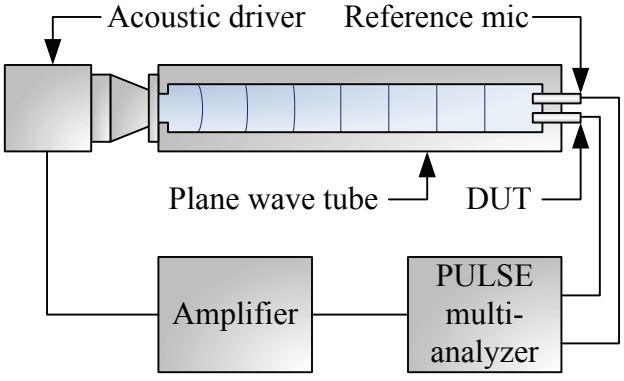

Figure 4. Experimental setup for frequency response measurement in a plane-wave tube.

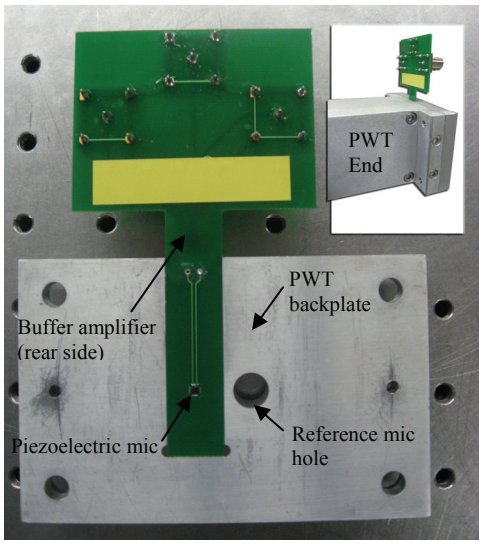

Figure 5. Packaged microphone, also shown mounted in plane wave tube (inset).

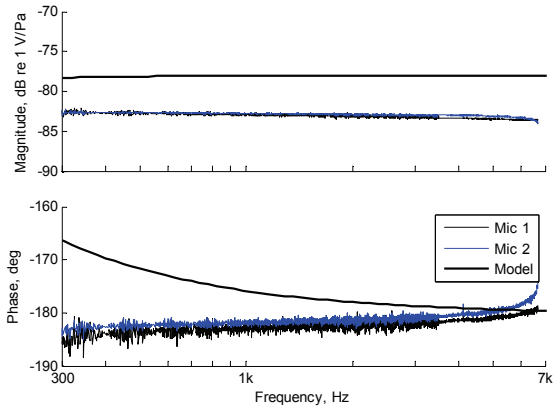

Figure 6. Measured microphone frequency response.

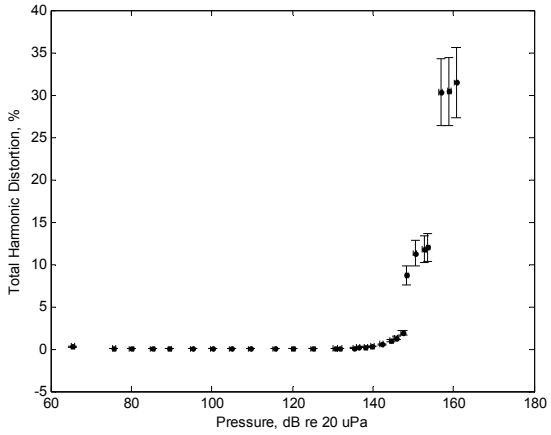

Figure 7. Total harmonic distortion for a 1 kHz tone, considering 5 harmonics.

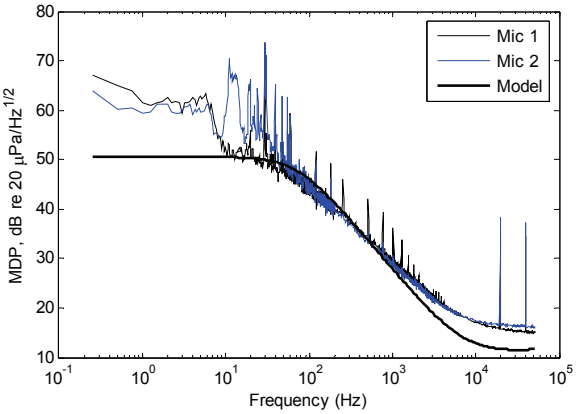

Figure 8. Measured and theoretical minimum detectable pressure (voltage noise referred to input via sensitivity at 1 kHz).

CONCLUSIONS

The design, optimization, and characterization of an AlN-based piezoelectric MEMS microphone for aeroacoustic measurements were described in this paper. This microphone is among the earliest to use AlN over more common piezoelectrics such as PZT and ZnO, and is the first targeted at aeroacoustic applications. Characterization of two AlN-based microphones yielded a sensitivity of 71 μV/Pa , dynamic range of 29-147 dB SPL, and resonant frequency of 89 kHz.

A comparison of experimental results with those from prior piezoelectric mics is found in Table 1. The sensitivity of the microphones presented here (71 μV/Pa), though lower than the two prior AlN-based microphones [12-13] (180 μV/Pa and 2 mV/Pa), was more than an order of magnitude better than the most recent piezoelectric aeroacoustic microphone [10]. The noise floor was also improved, and was comparable to that reported in [12]. Finally, the resonant frequency of 89 kHz is the highest reported among piezoelectric microphones, indicating a particularly large useable bandwidth.

Table 1: Summary and comparison with previous work.

Researcher	Material	Sensitivity (mV/Pa)	f_{res} (kHz)	*MDP* (dB SPL)	*PMAX* (dB SPL)
Present work	AlN	0.071	89	29[a], 64[b]	147
Littrell et al. [12]	AlN	0.18	11	58[b]	148
Fazzio et al. [13]	AlN	0.5-2	NR	NR	NR
Horowitz et al.[10]	PZT	0.0017	59	35.7[a], 95.3[b]	169
Kim et al. [5]	ZnO	1	16	50[b]	NR
Ried et al. [6]	ZnO	0.92	18	57[b]	NR
Lee et al. [8]	ZnO	30	0.89	NR	NR
Royer et al. [4]	ZnO	0.25	10	66.02[c]	NR
Schellin et al. [7]	Polyurea	0.030	NR	NR	NR
Ko et al. [9]	ZnO	0.51[d]	7.3	NR	NR

[a] At 1 kHz w/ 1 Hz bin; [b] A-weighted; [c] Method not reported; [d] At resonance

For future work, agreement between the model and experiment can be improved. The discrepancies are believed to relate to uncertainty in residual stresses and thin film properties, and efforts are currently underway to establish the source of disagreement. Other ongoing efforts involve improving the test package and characterization of a new round of devices. Finally, future microphone designs with lower noise floors may be achievable via careful design of the piezoelectric layer such that 1/f noise is pushed out of the audio band.

ACKNOWLEDGEMENTS

Fabrication was performed by Avago Technologies of Fort Collins, CO. Financial support for this work was provided by Boeing Corporation and a NSF Graduate Fellowship.

REFERENCES

[1] B. Burnett "Ssshh, we're flying a plane around here," Boeing Frontiers, vol. 4, 2006.

[2] V.G. Mengle et. al., "Clocking effects of chevrons with azimuthally-varying immersions on shockcell/cabin noise" 29th AIAA Aeroacoustics Conference, #08-3000, Vancouver, British Columbia Canada, 2008.

[3] I.C. Organization, "Occupational safety and health protections for cabin crew members," 36th Assembly of the International Civil Avation Organization, A36-WP/208, Montreal, Canada, 2007.

[4] M. Royer et al., "ZnO on Si integrated acoustic sensor," Sensors and Actuators, vol. 4, 1983, pp. 357-362.

[5] E.S. Kim, J.R. Kim, and R.S. Muller, "Improved IC-compatible Piezoelectric Microphone and CMOS Process," International Conference on Solid-State Sensors and Actuators, San Francisco, CA, 1991, pp. 270-273.

[6] R. Ried, D. Hong, and R. Muller, "Piezoelectric microphone with on-chip CMOS circuits," J. Microelectromech. S., vol. 2, 1993, pp. 111-120.

[7] R. Schellin, G. Hess, R. Kressmann, and P. Wassmuth, "Micromachined silicon subminiature microphones with piezoelectric P(VDF/TRFE)-layers and silicon-nitride-membranes," 8th International Symposium on Electrets, 1994, pp. 1004-1009.

[8] S.S. Lee, R.P. Reid, and R.M. White, "Piezoelectric Cantilever Microphone and Microspeaker," Journal of Microelectromechanical Systems, vol. 5, 1996, pp. 238-242.

[9] S.C. Ko, Y.C. Kim, S.S. Lee, S.H. Choi, and S.R. Kim, "Micromachined piezoelectric membrane acoustic device," Sensor. Actuat. A-Phys, vol. 103, 2003, pp. 130-134.

[10] S. Horowitz, T. Nishida, L. Cattafesta, and M. Sheplak, "Development of a micromachined piezoelectric microphone for aeroacoustics applications," J. Acoust. Soc. Am., vol. 122, 2007, pp. 3428-3436.

[11] S. Trolier-McKinstry and P. Muralt, "Thin Film Piezoelectrics for MEMS," J. Electroceram., vol. 12, 2004, pp. 7-17.

[12] R. Littrell and K. Grosh, "Advantages of piezoelectric MEMS microphones," 157th Meeting of the Acoustical Society of America, Portland, OR, 2009.

[13] R.S. Fazzio et al., "Design and Performance of Aluminum Nitride Piezoelectric Microphones," Solid-State Sensors, Actuators and Microsystems Conference, 2007, pp. 1255-1258.

[14] S.D. Senturia, "Microsystem Design," Kluwer Academic Publishers, 2001.

[15] S.A. Prasad et al., "Analytical electroacoustic model of a piezoelectric composite circular plate," AIAA Journal, vol. 44, 2006, pp. 2311-2318.

[16] G. Wang, B.V. Sankar, L.N. Cattafesta, and M. Sheplak, "Analysis of a composite piezoelectric circular plate with initial stresses for MEMS," ASME International Mechanical Engineering Congress, New Orleans, LO, United States: ASME, 2002, pp. 339-346.

CONTACT

*M. Sheplak, tel: +1-352-392-3983; sheplak@ufl.edu